The influence of temperature on the structural, morphological, optical, electrical, hemocompatibility and magnetic characterization of CoFe$_2$O$_4$ nanostructures

J. GAJENDIRAN[a,*], V. P. SENTHIL[b], J. RAMANA RAMYA[c], N. SIVAKUMAR[d], T. SHANMUGAVEL[e],
S. GOKUL RAJ[f,*], G. RAMESH KUMAR[g]

[a]*Department of Physics, Vel Tech Rangarajan Dr.Sagunthala R&D Institute of Science and Technology, Avadi, Chennai 600 062, India*
[b]*Naval Unit NCC, 2TN, Madurai-625017, India*
[c]*National Center for Nanoscience and Nanotechnology, University of Madras, Chennai, India*
[d]*Crystal Growth Centre, Anna University, Chennai-600 025, India*
[e]*Department of Physics, Mahendra Engineering College, Mallasamudram, Namakkal – 637 503, India*
[f]*Department of Physics, C. Kandaswami Naidu College For Men, Anna Nagar, Chennai, 600 102, India*
[g]*Department of Physics, University College of Engineering Arni, Anna University Chennai, Thatchur, Arni – 632 326, India*

A plausible formation mechanism of metal nitrate-citrate sol-gel synthesis CoFe$_2$O$_4$ nanostructures has been successfully proposed. To date, there is no report on the effect of calcination's temperature on the microstructural, optical and hemocompatibility properties of CoFe$_2$O$_4$ nanoparticles is investigated comparatively in detail using the W-H plot, FE-SEM and TEM, UV-visible and hemocompatibility analysis. In addition, the electrochemical, magnetic and dielectric properties of CoFe$_2$O$_4$ nanoparticles calcined at 800°C was characterized by the CV, LT-VSM and impedance analysis. The band gap of CoFe$_2$O$_4$ nanoparticles was calculated to be around 1.89, 1.84 and 1.77 eV for 600, 700 and 800°C, respectively.

1. Introduction

Cobalt ferrite (CoFe$_2$O$_4$) nanostructures finds for potential applications such as magnetic storage device, spintronics and electrical insulating devices due to their high magnetic moment, better inter-particles interaction, distribution of magnetic anisotropy, and redistribution of cation ions at low temperature and high temperature magnetization, Mossbauer and impedance measurements. Moderate magnetic saturation, high coercivity, very high dielectric constant give us an added advantage for improved electrical resistivity and low thermal conductivity in addition to good chemical stability and mechanical durability etc [1-6].

Preparation of gadolinium (Gd) doped CoFe$_2$O$_4$ nanoparticles by using the solid state ceramic route has been reported by Rahman et al. [7]. They reported on the changes of bulk grain and grain-boundary involvements movement the electrical resistance of CoFe$_2$O$_4$ material dependent on temperature. Ramana et al.[8] have reported on manganese (Mn) doped CoFe$_2$O$_4$ nanoparticles by using the solid state method. They reported on the tuning of structural, magnetic, and dielectric properties in doped CoFe$_2$O$_4$.Vaithyanathan et al. [9] have reported the structural characterization, temperature, and frequency dependent dielectric studies of undoped and titanium (Ti) doped CoFe$_2$O$_4$ nanoparticles by the solid state method.

The development of grain boundary conduction with respect to temperature increase has been reported from impedance studies. Mund et al. [10] have reported the CoFe$_2$O$_4$ nanoparticles by the solid state method in which the orbital magnetization in CoFe$_2$O$_4$ using magnetic Compton profiles was discussed in detail. The tuning of magnetic and dielectric properties of CoFe$_2$O$_4$ nanoparticles was synthesized by the gel combustion technique by the use of iron nitrate (Fe (NO$_3$)$_3$.9H$_2$O) and cobalt carbonate (CoCO$_3$) in the presence of potassium chloride (KCl), and glycine as a combustion agent by Vasundhara et al. [11]. Xavier et al. [12] have reported that CoFe$_2$O$_4$ nanostructures through were prepared via the sol-gel synthesis method by using cobalt nitrate and ferric nitrate dissolved in ethane diol and reported on the effect of the structural, dielectric and electric conductivity properties of cobalt ferrite (CoFe$_2$O$_4$) nanoparticles due to high temperature calcinations. Yadav et al. [13] have reported on the monosaccharide assisted sol-gel combustion route of CoFe$_2$O$_4$ nanoparticles synthesized and also presented the size dependent structural, magnetic, dielectric and electrical properties. Vadivel et al. [14] have investigated on the influence of sodium dodecyl sulfate (SDS) concentration on the phase purity, average crystallite size, lattice constant, morphological, dielectric and magnetic parameters of CoFe$_2$O$_4$ nanoparticles by the co-precipitation route. Prabhakaran et al. [15] have

reported the preparation of $CoFe_2O_4$ nanoparticles by the combustion route using cobalt nitrate and iron nitrate in the presence of amino acid (alanine). The influence of calcinations temperature on the structural parameters, phase identification, crystallinity, microstructures and magnetic parameters properties were reported them. Khandekar et al. [16] have comparatively investigated the influence of calcinations temperature on the particle size and DC resistivity, dielectric constant and AC conductivity studies of $CoFe_2O_4$ nanoparticles by the combustion route in the presence of base compounds in the nitrate counterparts of cobalt nitrate and iron nitrate with hexamine as a complexing (binding) agent. Moayyer et al [17] have reported the preparation of $CoFe_2O_4$ nanoparticles via the solid state method and explored the tuning of the crystal phase transformation $CoFe_2O_4$ nanoparticles from the Co_3O_4/Fe_2O_3 with respect to calcinations temperature. There were also few other report on the tuning of average particle size, strain, lattice constant, saturation magnetization and coercivity values of $CoFe_2O_4$ nanoparticles by the sol-gel or auto-combustion methods dependent on different calcinations temperature [18-20]. The crystalline nature, microstructure, particle sizes, photoluminescence and optical energy band gap, saturation magnetization, coercivity and remanent magnetization values of $CoFe_2O_4$ nanoparticles via the conventional heating and microwave heating methods have been comparatively investigated by Kombaiah et al. [21]. PEG assisted cobalt ferrite ($CoFe_2O_4$) nanoparticles via the solution combustion method and their electrochemical performances have been investigated by Vijaya Sankar et al. [22]. Various literatures reported on particle size, crystallinity and phase purity due to which there were reports on increased saturation magnetization, coercivity, dielectric constant, lesser dielectric loss and improved electrical resistivity values of the cobalt ferrite are highly dependent on the various synthesis methods. The present investigation metal nitrate-citrate- sol-gel combustion method emphasizes the merits such as homogeneous mixing of the starting metal nitrate salts of cobalt nitrate and iron nitrate in a aqueous solvent, uniform mixing of nitrates to produce phase pure compound from the homogeneous mother solvent in a short period of synthesis and easy scale up to the nano regime.

To date, there is no report on the effect of calcinations temperature on the structural, morphological, optical, and hemocompatibility properties of $CoFe_2O_4$ nanoparticles have been comparatively discussed by the combustion of metal nitrate-citrate sol-gel synthesis method with the help of W-H, FE-SEM, TEM, UV-visible and blood compatibility experiment analysis. Moreover, elemental composition, electrochemical, magnetic, and cation distribution with the help of EDX, CV, LT-VSM (Field cooled and Zero-field cooled (FC/ZFC) magnetic measurement) curve and Mossbauer spectrum analysis of $CoFe_2O_4$ (CFO) nanoparticles calcined at 800 °C have been investigated. An elaborated discussion of the frequency and temperature effect of the dielectric properties on the $CoFe_2O_4$ nanoparticles calcined at 800 °C was carried out by the impedance analysis.

2. Experimental section

Recently, we reported the single phase $CoFe_2O_4$ (CFO) nanoparticles were synthesized by using iron nitrate ($Fe(NO_3)_3 \cdot 9H_2O$) and cobalt nitrate ($Co(NO_3)_2 \cdot 6H_2O$) salts with citric acid as a fuel ($C_6H_8O_7$) in the presence of aqua (H_2O) solvent via themetal nitrate-citrate sol-gel combustion [3]. In the earlier work, we reported only the experimental procedure for preparation and schematic formation mechanism of $CoFe_2O_4$ nanoparticles and its magnetic properties. In this present work, we have successfully explained the formation of $CoFe_2O_4$ nanoparticles through chemical reaction and report on the electrical properties. Initially, the unstable metal aqua complex formed; when the metal salts such as iron nitrate and cobalt nitrate are mixed with aqua. After hydrolysis, citric acid ($C_6H_8O_7$) introduce into the metal nitrate solution, citrate-metal (chelate-metal) complex being formed [23-25]. Then, the citrate-metal complex sol is changed to gel due to the slowly evaporating solvent (aqua), leading to the formation of a viscous gel network. Then, the obtained viscous gel network dried and followed by calcined at 600, 700 and 800° C, which produces $CoFe_2O_4$ in the nanoparticles regime. Preparation of $NiFe_2O_4$ particles through the chemical reaction of nickel nitrate and ferric nitrate salts with citric acid in the presence of water have been reported by Prasanna et al. [26]. We think that the formation mechanism of the $CoFe_2O_4$ nanoparticles in our method would be same to that reported by Prasanna et al, except that cobalt nitrate was used instead of nickel nitrate.The formation mechanism of the cobalt ferrite nanoparticles is given below:

$$Co(NO_3)_2 \cdot 6H_2O + 2\ Fe(NO_3)_3 \cdot 9H_2O + C_6H_8O_7 \rightarrow sol\text{-}gel \rightarrow CoFe_2O_4 + CO_2 + NO + H_2O \qquad (1)$$

Williamson-Hall (W-H) method was adopted for calculating the particle sizes of nanocrystalline cobalt ferrite powders from the powder X-ray diffraction (XRD) results which was obtained from the Rigaku powder X-ray diffractometer with Cu-Kα radiation of wavelength (λ = 1.5406 Å). The particle morphology was found with the help of Field Emission Scanning Electron Microscopy (FEI Quanta FEG 200) with Energy Dispersive X-ray (EDX), and Transmission Electron Microscopy (TEM, H8100, Hitachi, Japan) analysis. The optical energy band gap was calculated by the UV-Visible (Jasco V-760 UV-Visible spectrometer) spectra. The cyclic voltametry (CV) was performed with the help of the Biologic SB150.The electrochemical consisted of glassy carbon electrode (GCE), silver/silver chloride as a reference electrode and platinum as the counter electrode. 10 mg of $CoFe_2O_4$

samples were dispersed in 5 mL of acetone. After that, the working electrode was prepared by coating (GCE) containing a mixture of the active material. Finally, three electrode configurations are fixed in 1M of potassium hydroxide (KOH) aqueous electrolyte. The Vibrating Sample Magnetometer (VSM) (Lakeshore, USA) was performed to discuss the magnetic nature and magnetic phase transition of the $CoFe_2O_4$ sample at low temperature magnetic measurement. Mossbauer data were observed with the help of a Canberra S-100 spectrometer using a $_{57}Fe$ source.The dielectric properties were measured by using Solartron Impedance Analyzer.

3. Results and discussion

The crystallographic parameters of crystal structure, average crystallite size, lattice constant and strain was used to discuss with the help of powder XRD data for obtained cobalt ferrite calcined samples. From the powder XRD pattern, Full Width Half-Maximum (FWHM), diffraction planes and the corresponding (hkl) planes were indexed for cobalt ferrite ($CoFe_2O_4$) samples and it is shown in Table.1.

The strongest reflection plane (311) of Full Width Half-Maximum (FWHM) values is smaller when calcined at 800 °C when compared to $CoFe_2O_4$ samples calcined at 600°C and 700°C. Generally, an increase in the average crystallite size of $CoFe_2O_4$ with respect to the increased calcinations temperature due to the FWHM decrease with an increase of calcined temperature. A careful examination of the XRD data reveals the appearance of slightly narrow peaks (not shown in Figure) signifying the larger grain size of the higher calcined sample due to grain growth. In addition, the Bragg reflection from the (111), (220), (311), (222), (400), (422), (511) and (440) planes correspond to pure $CoFe_2O_4$ samples with a cubic system with spinel structure from the powder XRD data and thus the lattice parameter values estimated from the XRD data was in good agreement with that of our earlier reports [3].
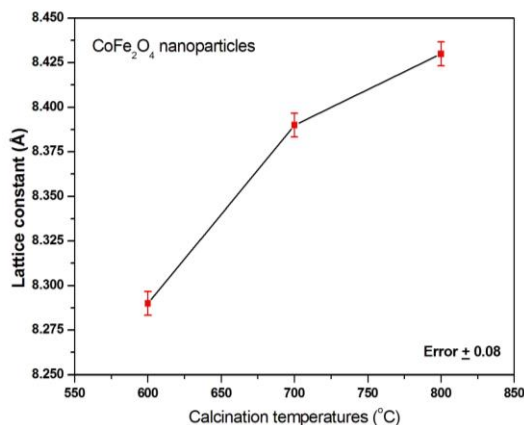
Fig. 1. a Lattice constant with calcination temperature for $CoFe_2O_4$ nanoparticles (color online)

The lattice constant was found from the XRD peak of the (311) plane by using the relation lattice constant $(a) = d / \sqrt{(h^2 + k^2 + l^2)}$ is thus values in Table 2, where, d is the interplanar distance and (hkl) represents the corresponding Miller indices. The lattice constants of the $CoFe_2O_4$ samples have been observed as 8.29 Å, 8.39 Å and 8.43 Å from the strongest peak of (311) for 600 °C, 700 °C and 800 °C, respectively which possesses the similar values, which is in good agreement with that of previous reports [8,18]. The lattice constant versus calcined temperature is shown in Fig.1a and it reveals that the lattice constant is increased with an increase in calcined temperatures leading to the coalescence of the smaller size particles which is due to the thermal stress induced between the metal oxide bonding.

Moreover, the interplanar distance for the corresponding plane values are given in Table.2. The average crystallite size and induced strain of $CoFe_2O_4$ samples is measured by the use of Williamson-Hall (W-H) plot [27- 29].

Table 1. 2θ, (hkl) and FWHM obtained from the XRD pattern of the cobalt ferrite

(hkl)	2θ	FWHM (radian)		
		600°C	700°C	800°C
(111)	18.4°	0.272	0.181	0.248
(220)	30.4°	0.318	0.195	0.217
(311)	35.9°	0.39	0.19	0.21
(222)	37.2°	0.374	0.439	0.31
(400)	43.3°	0.434	0.224	0.34
(422)	53.8°	0.37	0.28	0.239
(511)	57.4°	0.503	0.287	0.359
(440)	62.7°	0.51	0.342	0.333

The W-H method using the relation according to the Uniform Deformation Model (UDM) is given in the equation below.

$$\beta\cos\theta = K\lambda/D + \varepsilon\,(4\sin\theta) \tag{2}$$

A plot between $\beta\cos\theta$ and $4\sin\theta$ is a linear line shown in Fig. 1b. The size and strain line respectively by using linear fit equation (2) indicate the UDM.

From the graph, it can be seen that $\beta\cos\theta$ and $4\sin\theta$ yielded a straight line and that the intercept and slope of $CoFe_2O_4$ at different calcined temperatures are listed on Table 3. A positive slope is observed for the $CoFe_2O_4$ samples from the W-H plot which confirms the presence of a tensile strain that would be correlated to the crystal lattice disturbance because thermal effects [28]. From the UDM was observed the isotropic behavior of the obtained samples due to which all the sample properties are free of direction. The strain (ε) values of $CoFe_2O_4$ are found to be 0.124, 0.098 and 0.085 for 600 °C, 700 °C and 800 °C, respectively from the slope of the plots. When a small strain attributed to an increase crystallite size and a large strain is attributed to a small crystallite size [29]. The higher calcinations temperature, larger will be crystallite

size due to which strain values gradually decrease as a function of calcinations temperature

Table 2. Interplanar distance (d space) values of the cobalt ferrite at different calcined samples

(hkl) plane	d-spacing (A°)		
	600°C	700°C	800°C
(111)	4.759	4.786	4.860
(220)	2.934	2.989	2.970
(311)	2.503	2.513	2.530
(222)	2.395	2.457	2.410
(400)	2.077	2.120	2.080
(422)	1.698	1.713	1.711
(511)	1.604	1.614	1.610
(440)	1.473	1.482	1.481

Fig. 1c shows the influence of the calcined temperature on the tuning of average crystallite size of the $CoFe_2O_4$ samples. The average crystal size was determined from the W-H plot and it was found that the average crystallite sizes of the $CoFe_2O_4$ samples changes between 40 to 80 nm when the calcinations temperature increased from 600 °C, 700 °C and 800 °C and thereby from the plot the estimated crystallite size is listed in Table 4 in which the lattice constant is also provided. Thus, the obtained result is in good consistent with that of the values reported elsewhere by our group had previously which was estimated from simple Debye Scherrer's formula calcined at various temperatures from the XRD pattern [3].
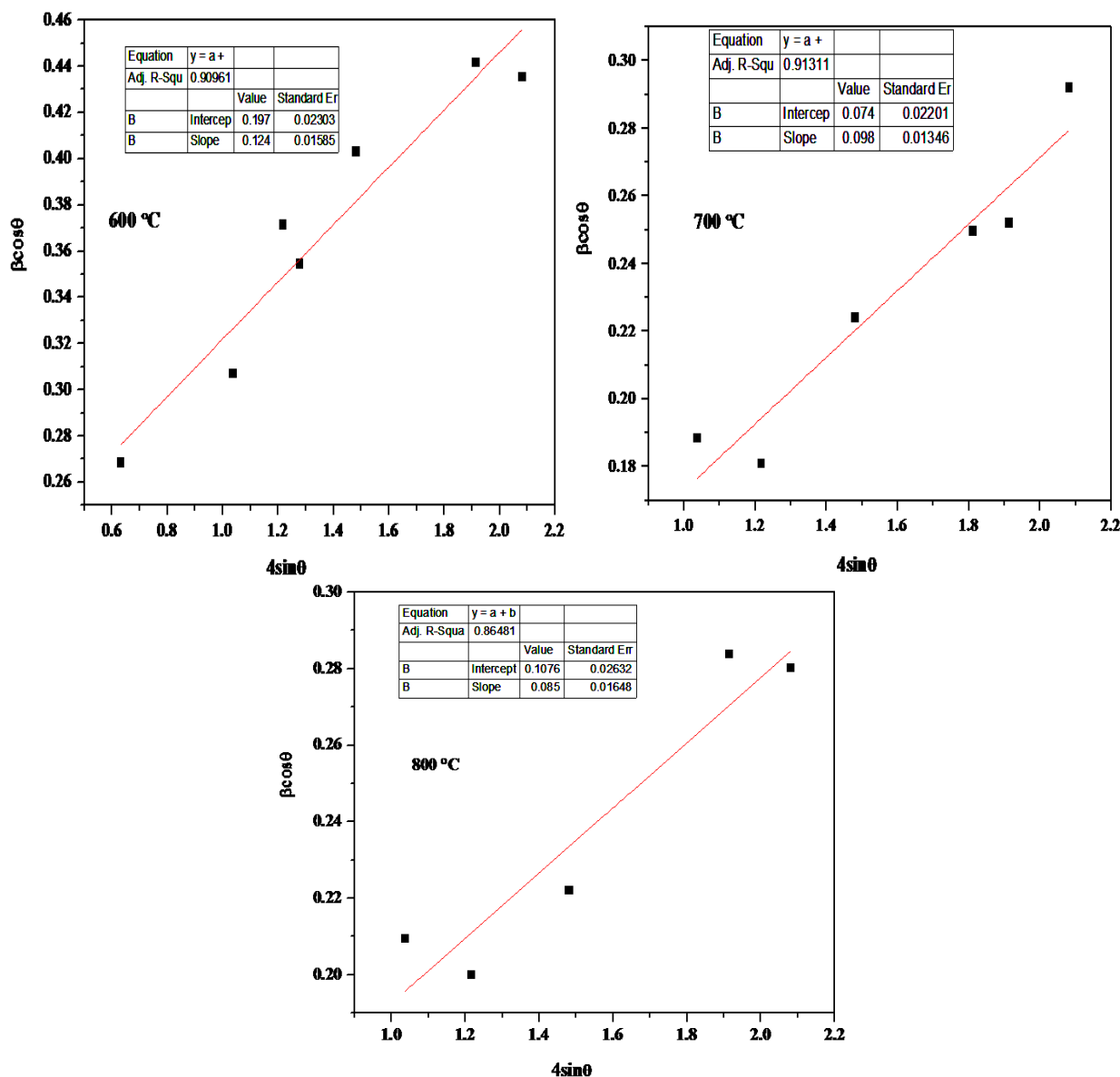
Fig. 1. b W-H Plot of CoFe2O4 samples calcined at 600°C, 700 °C and 800 °C (color online)
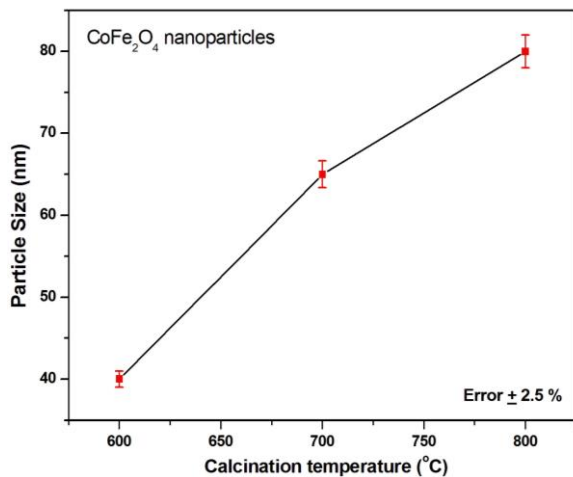
Fig. 1. c Crystallite size of CoFe₂O₄ samples calcined at 600 °C, 700 °C and 800 °C (color online)

Table 3. Intercept and slope of the cobalt ferrite powder at different calcined samples

$CoFe_2O_4$ Samples	600°C	700°C	800°C
Intercept	0.197	0.074	0.107
Slope	0.124	0.098	0.085

Table 4. Unit cell parameters of the cobalt ferrite powder calcined and average crystallite size at different calcined temperatures

$CoFe_2O_4$ Samples	Average Crystallite size (nm)	Lattice constant (Å)
600 °C	40	8.29
700 °C	65	8.39
800 °C	80	8.43

The particle surface structure of the $CoFe_2O_4$ (CFO) samples are examined by the FE-SEM studies (Fig.2 (a-c)). It can be clearly observed that almost aggregated spherical particles. Moreover, it shows the grains of various sizes, which were spread throughout the nanocrystalline CFO surface. We are unable to measure particle size of CFO samples in the FE-SEM images due to the aggregated particles. When these CFO samples were examined under Transmission Electron Microscopy (TEM), we could measure the particle size of the CFO samples.
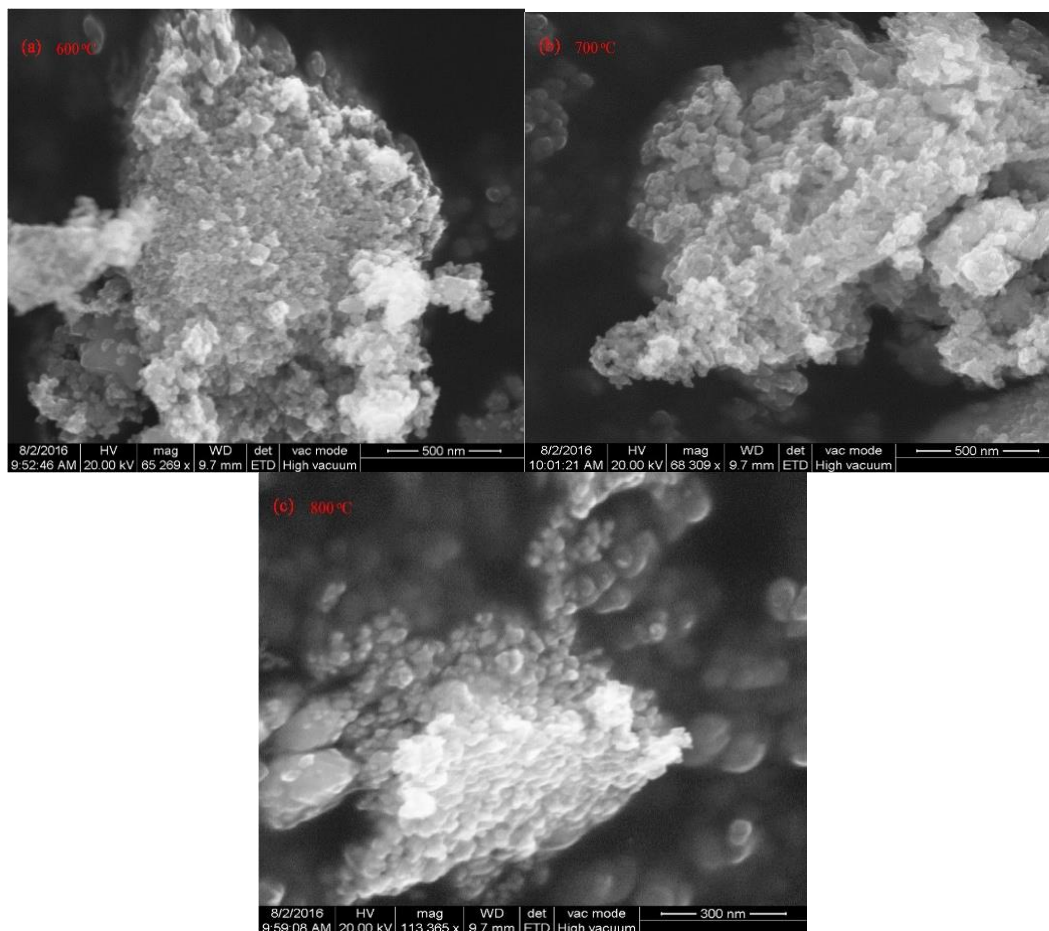
Fig. 2. FE-SEM images of CoFe₂O₄ nanoparticles calcined at 600 °C, 700° C and 800°C (color online)

The particle shape and size of $CoFe_2O_4$ samples are examined by the TEM studies. There is less agglomeration is much higher in the low-temperature calcined $CoFe_2O_4$ sample; however, the large agglomeration were observed with increasing of the calcinations temperature, due to the induced particle growth and that particle coalescence can be clearly observed in the TEM images (Fig.3(a-c)).

(a)

(b)

(c)
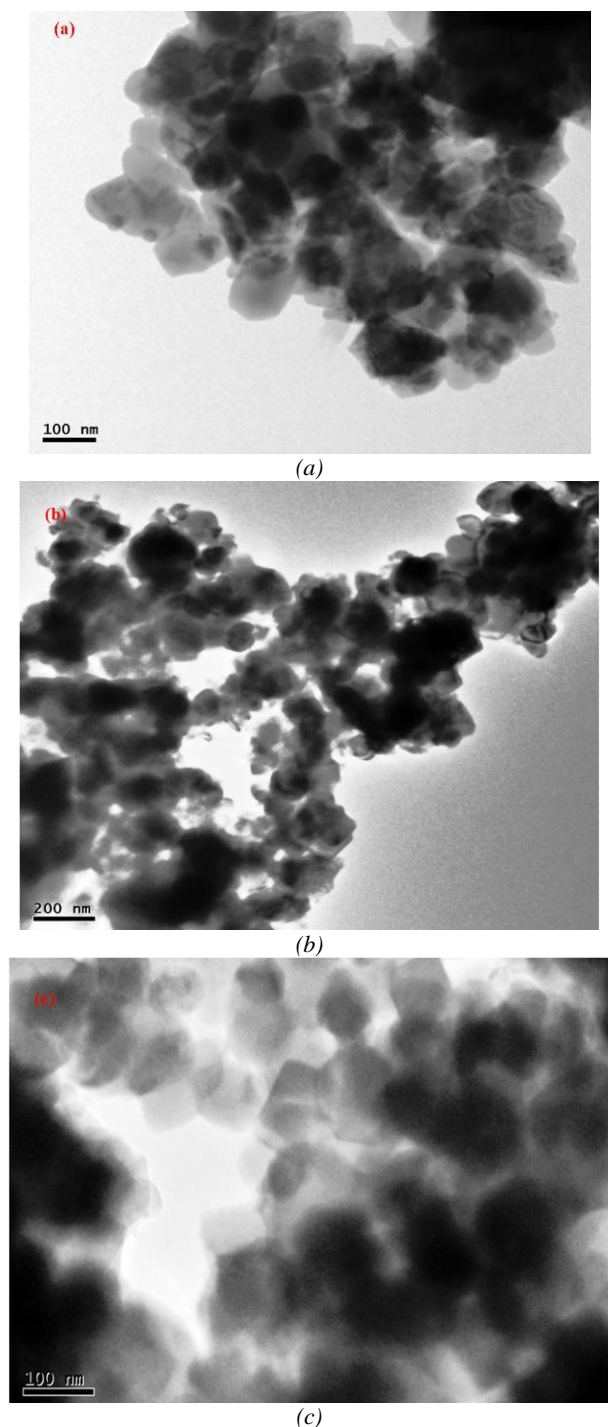
Fig. 3. (a-c) TEM images of the $CoFe_2O_4$ samples calcined at 600 ºC, 700 ºC and 800 ºC (color online)

From the Fig. 3 (a-c), the particle size of $CoFe_2O_4$ was measured to be around as ~ 50-55, 65-70 and 80-90 nm for the calcinations temperature of 600 ºC, 700 ºC and 800 ºC. Larger particles can be seen at higher calcined temperatures due to the coalescence for the smaller particles and as the thermal preservation temperature goes up, particle receives more energy leading to continuous grain growth. Moreover, the particle grain growth is developed at higher calcinations temperatures which is clearly seen as distinct grain boundaries in which the grains are appeared as densely packed. Moreover, it shows the polycrystalline behavior with grains of different particle sizes, which were spread throughout the nanocrystalline CFO sample surface. The High Resolution Transmission Electron Microscopy (HR-TEM) (Fig.3d) and Selected Area Electron Diffraction (SAED) (Fig.3e) image of $CoFe_2O_4$ calcined at 600 °C clearly shows the poly crystalline behavior (blue arrow in Fig.3d & e) due to the different lattice fringes and various diffraction circles.

(d)

(e)
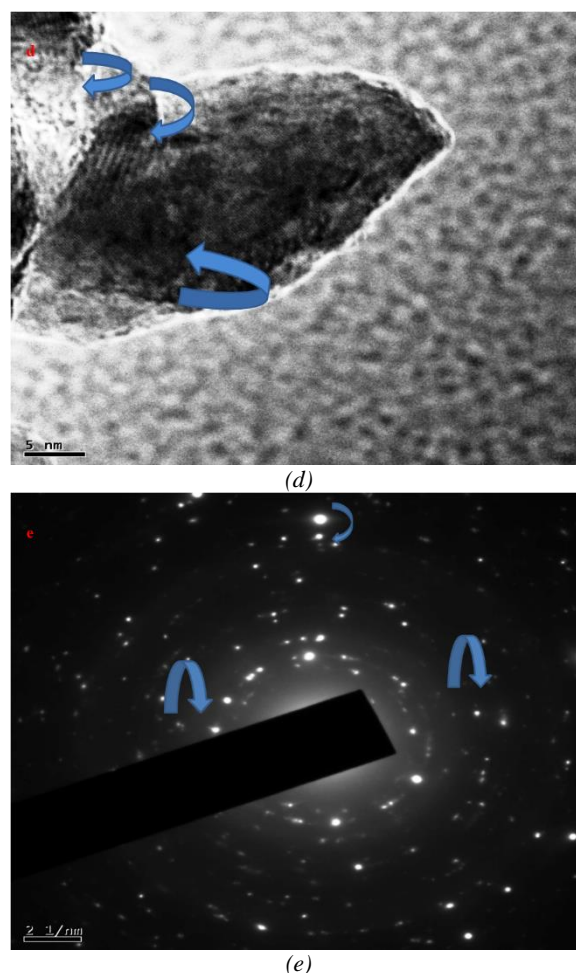
Fig. 3. (d) HR-TEM and (e) SAED images of the $CoFe_2O_4$ sample calcined at 600 ºC (color online)

The phase purity, and elemental analysis is done by the EDX analysis for determining the elemental composition of the $CoFe_2O_4$ sample calcined at 800 ºC is shown in Fig.4. From the EDX, we could observe the metals peak for Co, Fe and O peaks based on which the

EDX spectrum confirmed the corresponding metals in proper composition and thereby exhibiting the cobalt ferrite which is in agreement with that of the powder X-ray diffraction results of nanocrystalline cobalt ferrite. Moreover, the atomic percentage values are 14.1 %, 29 % and 56.9% for Co, Fe and O elements, respectively, which is evident that the sample has the exact stoichiometric ratio of $CoFe_2O_4$.
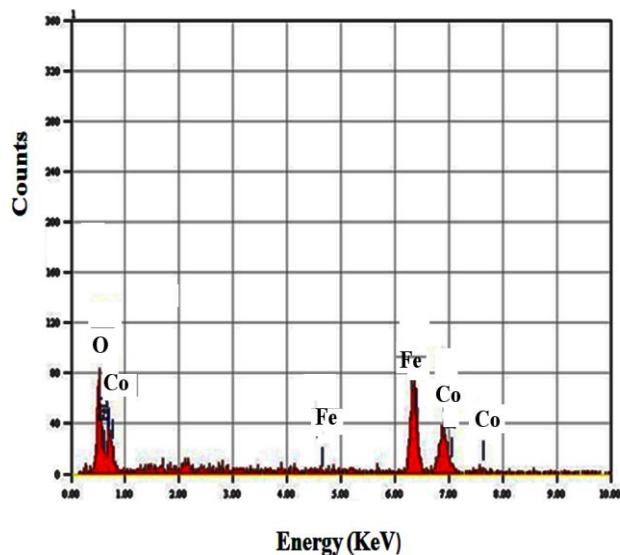
Fig. 4. EDX spectrum of the $CoFe_2O_4$ calcined at 800 ºC (color online)

The photo response interacting with the cobalt ferrite nanoparticles and its optical energy gap were examined by the UV-visible spectra. From the UV-visible spectra (Fig.5a), the optical absorption edge of the $CoFe_2O_4$ nanoparticles is clearly observed in the visible region due to the electron jumped from the ground state (valence band,VB) to the excited state (conduction band, CB). The absorption of light in the visible region is exhibited to the fundamental absorption of cobalt ferrite [21]. In addition, for the higher calcined $CoFe_2O_4$ sample, the optical absorption edge is shifted towards the longer wavelength in the visible region. Moreover, we can clearly see that, with increasing the calcination temperature the optical absorption decreases due to the following reasons:(i) narrow optical band gap and (ii) higher particle size. Because, $CoFe_2O_4$ has less suface to volume ratio and high inter particle distance athigher calcination temperature. So, the higher calcination temperature samples have less photoresponse.
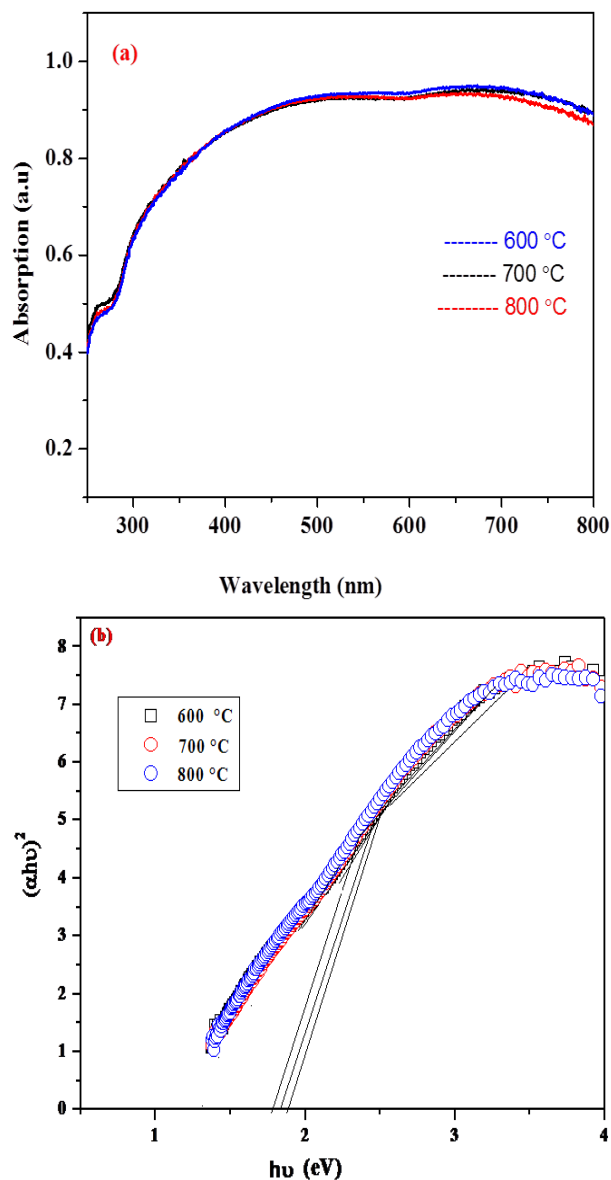
Fig. 5. (a) UV-Visible spectra and (b) Tau Davis Mott plots of $(\alpha h\upsilon)^2$ versus $h\upsilon$ of of $CoFe_2O_4$ nanoparticles calcined at 600 °C, 700 °C and 800 °C (color online)

The direct optical energy gap (E_g) of the $CoFe_2O_4$ nanoparticles is directly estimated from the Tau Davis Mott plot model. The Tau Davis Mott plot model extrapolating the graphs of $(\alpha h\upsilon)^2$ versus $h\upsilon$ is shown in Fig.5b. The optical band gaps (E_g) of the$CoFe_2O_4$ nanoparticles' values are found to be around 1.89, 1.84 and 1.77 eV for 600°C, 700°C and 800°C respectively. The observed E_g values of the $CoFe_2O_4$ samples can be used for nanoelectronic devices. Moreover, the red shift (decrease in optical band gap) is observed with increased calcinations temperature is observed from the Tau Davis Mott plot.

Thus, the red shift of the energy gap at higher calcination temperature may arise due to the development of crystallinity in the lattice due to which there is a decreased defect concentration in the $CoFe_2O_4$ sample. Generally, the energy gap of the nanoparticles samples is inversely proportional to the particle size and for present samples exhibited a reduced in the optical energy band gap for higher calcinations. Laokul et al. [30] have reported on the decreasing of optical band gap of $CoFe_2O_4$ samples with increasing calcined temperature, which is in consistent with our present work. Moreover, the decreasing band gap values of $CoFe_2O_4$ with respect to the increasing calcinations temperature are indirectly consistent with increasing average crystallite size of the $CoFe_2O_4$ samples with respect to increasing calcination temperatures from the Williamson-Hall plot.

The blood compatibility experiment was performed for the $CoFe_2O_4$ samples using human blood and stored in Sodium Heparin coated tubes which are pre-cooled at 4 °C. Firstly, the samples were sterilized for 1 h under ultraviolet (UV) radiation of 365 nm. The sterilized samples were equilibrated with 1 mL of saline solution in 5 mL centrifuge tubes and were incubated for one day at 37 °C. The saline was separate from the tubes and the collected human blood was added to the samples. The samples were incubated at 37 °C for few min. 2 mL of sterile saline was added and they were incubated for 1 h more. The tubes were centrifuged at 750 rpm for few min using the Remi R8C Centrifuge Machine. The serum was taken and stored in individual tube. The human blood with 2 mL of distilled water is the positive control and the human blood with 2 mL saline solution acts as the negative control. The optical density (OD) values were observed at 545 nm by using the Jasco V-760 UV-Vis Spectrophotometer. The percentage of hemolysis was measured using the relation given below,

$$\% \text{ of hemolysis} = \frac{\textbf{OD Value of the test sample} - \textbf{OD Value of the negative control}}{\textbf{OD value of the positive control} - \textbf{OD value of the negative control}} \text{ X } 100$$

The detected percentage of hemolysis for the $CoFe_2O_4$ samples was compared with the standard American Society for Testing and Materials (ASTM) values. The samples were reported strongly hemocompatible when the percentage of hemolysis was below 5%, whereas if it is between 5-10 % it was hemocompatible. If the hemolysis was greater than 20% it is non-hemocompatible [31, 32].

the nanoparticles which have a high dissolution rate [33]. Hence, the $CoFe_2O_4$ nanoparticles can be proposed for clinical procedures, such as drug delivery without damaging the blood capillaries and the blood composition [34].
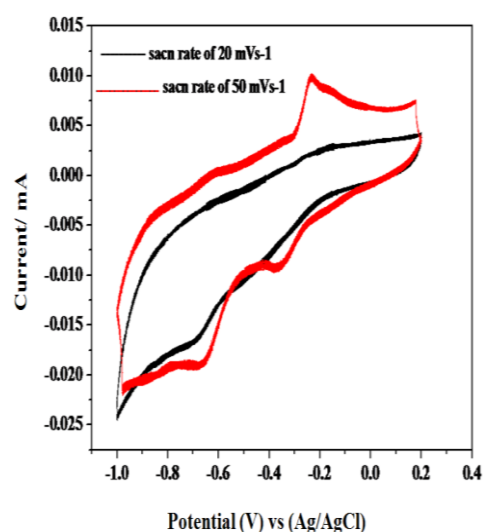
Fig. 7. CV curves of $CoFe_2O_4$ sample calcined at 800 °C scan rate at 20 and 50 mVs^{-1} (color online)

Fig. 6. Hemolytic assay of the $CoFe_2O_4$ samples (color online)

The hemocompatibility experiment was carried out for the $CoFe_2O_4$ (CFO) samples and the percentages of hemolysis were calculated (hemolytic activity). The obtained samples percentages of hemolysis values are in close agreement with the ASTM standards for obtained samples (Fig.6) [32, 33]. The $CoFe_2O_4$ samples showed less than 5% hemolysis representing a highly hemocompatible nature, which eventually indicates the lower toxicity level. This may be due to the smaller size of

The electrochemical property of the $CoFe_2O_4$ with modified electrode is examined by using the Cyclic Voltammetry (CV), measured in the between range of -1 to 0.2 V. The Cyclic Voltammetry of the $CoFe_2O_4$ electrode at the scan rate of 20 and 50 mVs^{-1} is shown in Fig.7. The $CoFe_2O_4$ sample's scan rate of 20 mVs^{-1} shown in the figure represents the rectangular curve that denotes it as the ideal capacitive behavior [35]. Moreover, electrostatic interaction or faradaic reaction on the electrode/electrolyte interface was observed in the CV curves. At 50 mVs^{-1}, $CoFe_2O_4$ exhibits two redox couples -0.63/0.6 V and -0.38/-0.16 V. The peak, E =-0.38 V is located on the

forward scan, and a small cathodic peak, -0.16 V is detected on the reverse scan. This redox couple is attributed to the Co^{+2}/Co^{+3} redox pair. On the other hand, -0.63/-0.6 V is ascribed to the iron species, ie.Fe^{+3}/Fe^{+2} redox reaction [36]. It shows that the charge is stored in the $CoFe_2O_4$ electrodes predominantly by this reaction and thus the redox peaks behavior in the CV curve demonstrates the pseudo capacitive nature of the $CoFe_2O_4$ [22]. As seen in the CV curves in the figure for $CoFe_2O_4$ at a scan rate of 50 mV s^{-1} covers a large area for the given voltage and output current, indicating the storage of high charge when compared to the scan rate of 20 mV s^{-1} which is the general feature of the voltammetry when the current is increased with respect to the scan rate [37]. The electrolyte ions are completely spread into the material at lower scan rates, and hence, they have sufficient time to utilize all the active sites of the electrode material for its use as charge storage. However, the movement of the electrolyte ions is limited by time constraints at higher sweep rates and only the outer active surface is used for charge storage which is based upon which it was ascertained that the synthesized $CoFe_2O_4$ on also scan rate.

The magnetic saturation, magnetic phase transition temperature, and magnetic blocking mechanism are described by the Low Temperature (LT) magnetic measurement. The LT magnetic measurement (Zero-field cooling (ZFC) and field cooling (FC) curve) of the $CoFe_2O_4$ nanoparticles calcined at 800°C is measured at 0-300 K (Fig.8a). The ZFC curve reveals that the magnetic saturation (M_s) value as 0.063 emu/g. whereas; the FC curve reveals the magnetic saturation value as 0.075 emu/g. We observed from the ZFC and FC curve of $CoFe_2O_4$ that as the temperature reduces from 300 to 0 K, the magnetization gradually increases. Finally, the magnetization decreases due to the increase in temperature, which the magnetic domain would be destroyed and thereby the alignment is perturbed. In addition, we observed the nodal shaped peak temperature at 35 K in both the ZFC and FC curves. This nodal shape peak reveals the magnetic phase transition temperature called blocking temperature (TB). The blocking temperature can be clearly seen at low temperature (15-50 K) in the inset in Fig.8a in which the TB attains the maximum saturation. Beyond a certain TB, the heat energy is more and thereby anisotropic energy due to the non uniform heat fluctuations causes decrease in magnetization.
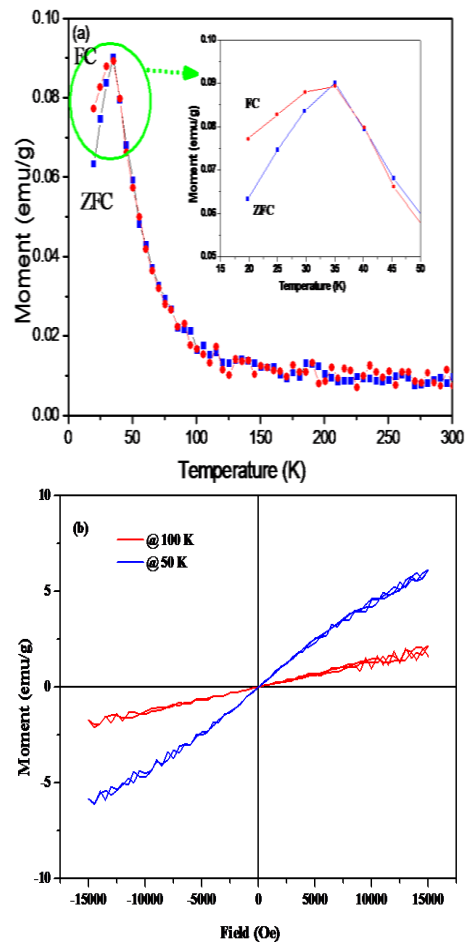
Fig. 8. (a) Low temperature (LT) magnetic measurement $CoFe_2O_4$ calcined at 800 °C and (b) LT-VSM of of $CoFe_2O_4$ sample at 100 K and 50 K for the sample calcined at 800 °C (color online)

The ZFC curve peak broadens which is due to the wider size distribution and more interaction among the nanoparticles. The observed of the broad peak at the ZFC curve can be attributed to the magnetic blocking mechanism induced by the competition between thermal energy and magnetic anisotropy energy. Below the blocking temperature the $CoFe_2O_4$ nanoparticles system goes into a disordered block state. As the temperature decrease from 300 to 35 K, the magnetic saturation increases which is due to the low temperature of the cobalt ferrite sample at lower field which in turn tries to align in the direction of the field [38]. Above the blocking temperature, the magnetic saturation of the $CoFe_2O_4$ nanoparticles system gradually is decreased due to its no longer being aligned towards the applied field and starts to become disoriented alignment which results in the decrease of magnetization. The reason is that thermal energy is sufficient to overcome the field-particle coupling. Based on the above observation, it can be correlated to the change in site occupancy which results in the highly influenced magnetic cations in ferrite structure [38].

Fig. 8b shows the M-H curve measured at 50 and 100 K, which reveals that the $CoFe_2O_4$ nanoparticles reveal

paramagnetism at low temperatures. We observed that the intensity of magnetization still remains unsaturated, even with the external applied field increasing up to 15 kOe which is due to the paramagnetic behavior of the $CoFe_2O_4$ nanoparticles. At 100 K, the coercivity and residual magnetism values are 14 Oe and 0.026emu/g, whereas, at 50 K, coercivity and residual magnetism values are 5 Oe and 79 emu/g and both the M-H curves have low coercivity and residual magnetism. We reported on the high temperature magnetic measurements [3] to determine the curie temperature of the $CoFe_2O_4$ nanocrystalline powder. In addition, the temperature dependent magnetic measurement was carried out for the $CoFe_2O_4$ samples calcined at 800 ºC and that the parameters of saturation magnetization (Ms) and coercivity (Hc) were reported recently at high temperatures [3].

The nuclear interaction and cation distribution properties of the $CoFe_2O_4$ nanoparticles are described by the Mossbauer spectrum is shown in Fig .9. We observed six lines in the Mossbauer spectrum because of Fe^{3+} ions at the tetrahedral and the other side due to Fe^{3+} ions at the octahedral site. We can clearly see that the cation exchange between the tetrahedral and octahedral sites of the as calcined sample at 800 °C is a significant factor which determined the magnetic properties. The obtained six line of the $CoFe_2O_4$ sample, which is in consistent with the tetrahedral and octahedral lattices which are characteristic of the spinel ferrite structures have been reported previously by Mazario et al. [39].
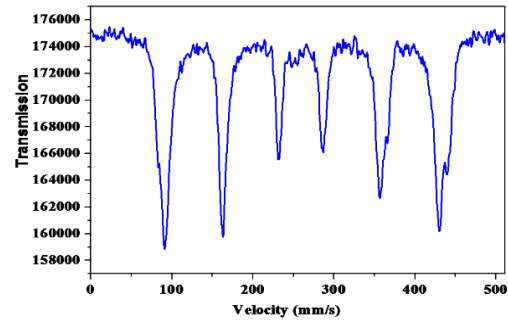
Fig. 9. Mossbauer spectrum of the $CoFe_2O_4$ sample at calcined at 800 ℃ (color online)

The dielectric constant, dielectric loss and electrical properties of $CoFe_2O_4$ nanoparticles were investigated by the impedance analysis. Tuning of the dielectric properties is dependent on frequency and temperature, and the results have been discussed in detail. Fig.10a reveals the tuning in the real part of impedance (Z') with respect to frequency (f) and temperature of the $CoFe_2O_4$ nanoparticles (calcined sample at 800 °C). It reveals that the value of Z' increases in the low frequency range and then Z' reduced with respect to increasing frequency except for 575 to 600°C.
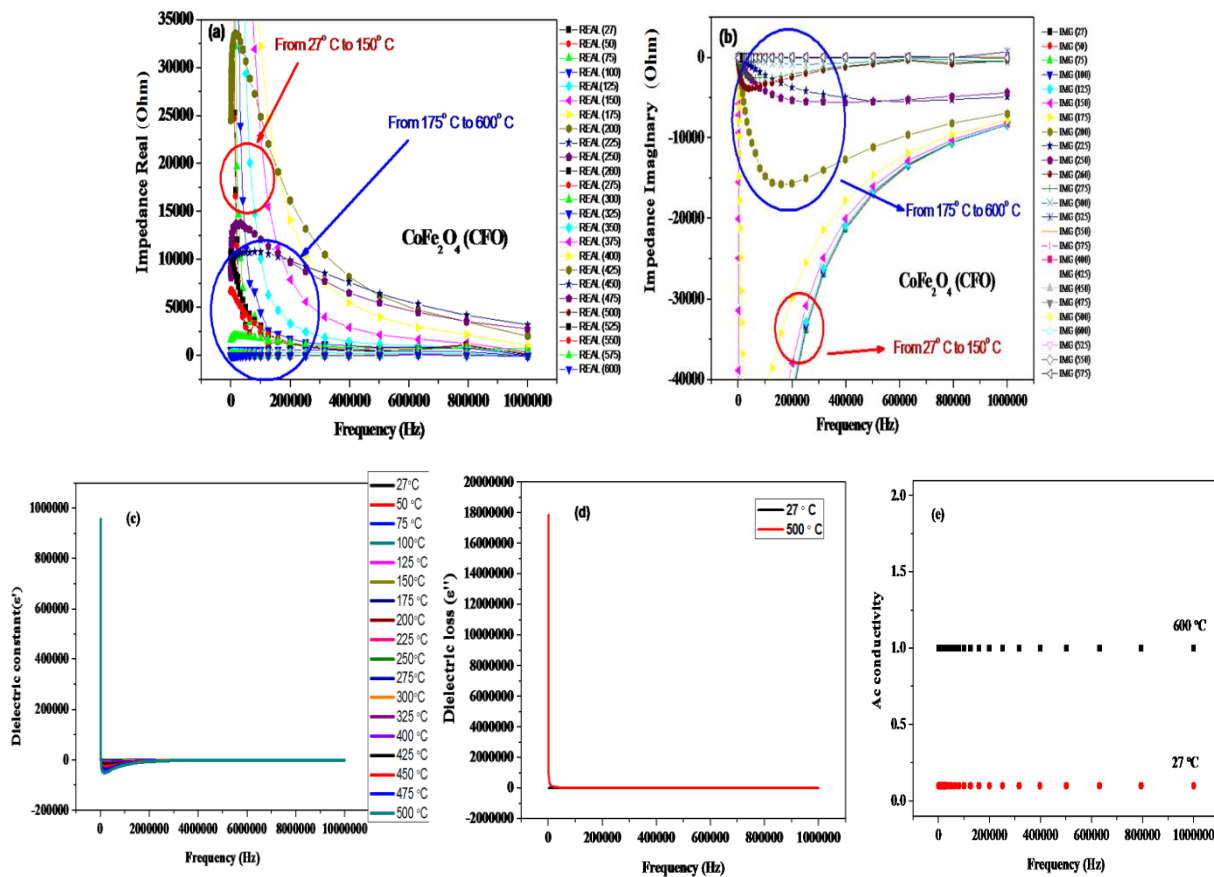
Fig. 10. (a) Frequency vs Impedance (real) for $CoFe_2O_4$ samples calcined at 800 ℃, (b) Frequency vs Impedance (imaginary) for $CoFe_2O_4$ samples calcined at 800 ℃, (c) Frequency vs Permittivity (real) for $CoFe_2O_4$ samples calcined at 800 ℃, (d) Frequency vs permittivity (imaginary) for $CoFe_2O_4$ samples calcined at 800 ℃ and (e) Frequency vs AC conductivity for $CoFe_2O_4$ samples calcined at 800 ℃ (color online)

The reduced in Z' as the frequency increased can be ascribed to the different types of polarization, such as electronic polarization, ionic polarization, orientational polarization and space charge polarization effect in the spinel ferrite structure nanoparticles [39]. The density of charge carriers in the space charge polarization depend on the frequency. Moreover, at low frequency from 27 to 150 °C, we observed that the impedance values are high, whereas, from 175 to 600 °C, the impedance values are low. The Z' values are high at low temperature with more number of atoms contribute to orientation polarization, which is inversely proportional to the temperature. Fig.10b reveals the changing in the imaginary part of impedance (Z'') with respect to the frequency of the $CoFe_2O_4$ calcined at 800°C. It also reveals that the value of Z'' increases in the low frequency part from 27 to 150 °C, whereas, Z'' slowly decreases at the low frequency of 175 to 600 °C and increases at a higher frequency. The changes of the dielectric constant (permittivity real) with respect to the frequency of the $CoFe_2O_4$ nanoparticles (sample calcined at 800°C) (Fig.10c) reveals that the dielectric constant value is reduced with respect to the increasing frequency and has become closely dielectric constant stable in the higher frequency part at all temperatures. The large value of the dielectric constant in the lesser frequency part is due to the increase in the polarization [2]. The constant value of the dielectric constant with increasing frequency is an actual dielectric activity of ferrite nanostructures [12].Commonly; dielectric materials have two different layers such as good conducting grain and poor conducting grain boundaries. These two different layers are separated by some distance in dielectric materials. In the lower frequencies part, high values of the dielectric constant were observed because of the grain boundaries. At lesser frequencies, the grain boundaries are dominant, whereas, at high frequencies region, grains are dominant. The obtained large value of the dielectric constant in the lower frequency part can be exhibited from the nano-sized particles compared to the bulk $CoFe_2O_4$ [40], because of the greater number of grains and grain boundaries present in the nano-sized particles. On the other hand, the electron does not synchronize with the applied electric field, beyond a certain boundary in the higher frequency part, and hence, the probability of electrons reaching the grain boundary reduces and thus decreases the resultant polarization. Maxwell-Wagner's two-layer and Koop's phenomenological theory [2, 13, 39, 40] have successfully explained the reduction in the dielectric constant with increase in frequency due to the space charge polarization effect. This effect may arise due to the frequency increasing the polarization of induced moments or electronic exchange between Fe^{+2} and Fe^{+3} ions not synchronizing with the frequency of the field [2, 9, 40, 41] and inhomogeneous structure of the dielectric materials. Moreover, the temperature dependence of the dielectric constant with respect to the frequency of $CoFe_2O_4$ nanoparticles (calcined sample at 800 °C) (Fig.10c) clearly reveals that the dielectric constant values gradually increases with increasing temperature because of the behavior of the polarization effect. Polarization is said to be weak, when the charge carriers does not orient themselves towards the direction of the applied electric current at low temperature, and hence the dielectric constant is low. Polarization is said to be strong, when the charge carriers get increased because of the increase in heat energy at high temperature, and this implies to an increase in the dielectric constant. The variations of dielectric loss (permittivity imaginary) with respect to the frequency at different temperatures of $CoFe_2O_4$ nanoparticles (calcined sample at 800 °C) are shown in Fig.10d. It reveals that the dielectric loss activity is close to that of the dielectric constant. The tuning of AC conductivity with respect to the frequency at room temperature and 600°C of $CoFe_2O_4$ nanoparticles (calcined sample 800°C) are shown in Fig.10e. From Fig.10e, AC conductivity exhibits constant with respect to frequency and it remains constant at 27 and 600 °C and hence, it is concluded due to small polarons. The dielectric and conductivity analysis confirm that $CoFe_2O_4$ can be used in high frequency applications.

4. Conclusions

The growth mechanisms of the $CoFe_2O_4$ nanoparticles via the metal-citrate sol-gel synthesis method successfully have been explained. The lattice constant of $CoFe_2O_4$ (CFO) decreases with increasing calcinations temperature from the powder diffraction data. FE-SEM and TEM images of the $CoFe_2O_4$ samples observed that spherical particles. The EDX and Mossbauer spectrum analysis confirm the presence of cobalt ferrite. The obtained narrow optical band gap (E_g) values of the$CoFe_2O_4$ samples can be used for photo catalytic, solar cell and opto-electronic devices. The $CoFe_2O_4$ samples revealed less than 5% hemolysis representing the highly hemocompatible nature. Based on the above results, we see that the tuning of sizes, optical band gap and hemolysis are under the influence of calcinations temperature. The$CoFe_2O_4$ electrodes at the scan rate of 50 mV s^{-1} were observed to have high charge storage compared to those at the scan rate of 20 mV s^{-1}from the CV analysis. The M-H curve measured at 50 and 100 K, reveals that the $CoFe_2O_4$ nanoparticles exhibit paramagnetism and it can be used for temporary magnetic devices and spintronics applications. Tuning of the dielectric properties was observed from the impedance analysis, to be dependent on frequency and temperature. Thus, the obtained $CoFe_2O_4$ nanomaterials can be used for high frequency applications.

project successfully in the DRDO-ARMREB sponsored facility.

References

[1] M. Sundararajan, L. JohnKennedy, Udaya Aruldoss, Sk. Khadeer Pasha, J. Judith Vijaya, Steve Dunn, Materials Science in Semiconductor Processing **40**, 1 (2015).

[2] T. Boobalan, N. Suriyanarayanan, S. Pavithradevi, Mater Sci. Semiconduc. Processing **16**, 1695 (2013).

[3] V. P. Senthil, J. Gajendiran, S. Gokul Raj, T. Shanmugavel, G. amesh Kumar, C. Parthasaradhi Reddy, Chem. Phys. Lett. **695**, 19 (2018).

[4] Shekhar D. Bhame, P. A. Joy, Chem. Phys. Lett. **685**, 465 (2017).

[5] S. M. Ansari, S. R. Suryawanshi, M. A. More, Debasis Sen, Y. D. Kolekar, C. V. Ramana, Chem. Phy. Lett. **701**, 151 (2018).

[6] S. Talukdar, D. Mandal, K. Mandal, Chem. Phys. Lett. **672**, 57 (2017).

[7] Md. T. Rahman, C. V. Ramana, J. Appl. Phys. **116**, 164108 (2014).

[8] C. V. Ramana, Y. D. Kolekar, K. Kamala Bharathi, B. Sinha, K. Ghosh, J. Appl. Phys. **114**, 183907 (2013).

[9] V. Vaithyanathan, L. N. Patro, Ugendar Kodam, H. Tan, S. S. R. Inbanathan, K. Kamala Bharathi, J. Appl. Phys. **118**, 114102 (2015).

[10] H. S. Mund, S. Tiwari, J. Sahariya, M. Itou, Y. Sakurai, B. L. Ahuja, J. Appl. Phys. **110**, 073914 (2011).

[11] K. Vasundhara, S. N. Achary, S. K. Deshpande, P. D. Babu, S. S. Meena, A. K. Tyagi, J. Appl. Phys. **113**, 194101 (2013).

[12] S. Xavier, M. K. Jiji, Smitha Thankachan, E. M. Mohammed, AIP Conf. Proc. **1576**, 98 (2014).

[13] R. S. Yadav, I. Kuřitka, J. Vilcakova, J. Havlica, J. Masilko, L. Kalina et al., Advances in Natural Sciences: Nanoscience and Nanotechnology **8**, 045002 (2017).

[14] M. Vadivel, R. Ramesh Babu, M. Arivanandhan, K. Ramamurthi, Y. Hayakawa, Ceramics International **42**, 14113 (2016).

[15] T. Prabhakaran, J. Hemalatha, Ceramics International **42**, 14113 (2016).

[16] M. S. Khandekar, R. C .Kambale, J. Y. Patil, Y. D. Kolekar, S. S. Suryavanshi, J. Alloys Comp. **509**, 1861 (2011).

[17] H. Akbari Moayyer, A. Ataie, Adv. Mater. Res. **829**, 767 (2014).

[18] K. S. Rao, G. S. V. R. K. Choudary, K. H. Rao, Ch. Sujatha, Procedia Mater. Sci. **10**, 19 (2015).

[19] Manju Kurian, Smitha Thankachan, Divya S. Nair, E. K. Aswathy Aswathy Babu, Arathy Thomas et al., J. Adv. Ceramics **4**(3), 199 (2015).

[20] J. B. Silva, Walter deBrito, Nelcy D. S. Mohallem, Mater. Sci. Eng. B**112,** 182(2004).

[21] K. Kombaiah, J. Judith Vijaya, L. John Kennedy, M. Bououdina, R. Jothi Ramalingam, Hamad A. Al-Lohedan, Ceramics International **43**, 682 (2017).

[22] K. Vijaya Sankar, R. Kalai Selvan, D. Meyrick, RSC Advances **5**(121), 99959 (2015).

[23] M. Sajjia, M. Oubaha, M. Hasanuzzaman, A. G. Olabi, Ceramics International **40**, 1147 (2014).

[24] Francesca Deganello, Materials Today Proceedings **4**, 5507(2017).

[25] Sagrario M. Montemayor, L. A. Garcıa-Cerda, J. R. Torres-Lubian, Materials Letters **59**, 1056 (2005).

[26] G. D. Prasanna, R. L. Ashok, V. B. Prasad, H. S. Jayanna, Journal of Composite Materials **49**(21), 2649 (2015).

[27] W. H. Abd. Majid, M. E. Abrishami, Ramin Yousef, A. Khorsand Zak, Solid State Science **13**, 251 (2011).

[28] K. Pradeev Raj, K. Sadayandi, Physica B: Physics of Condensed Mat. **487**, 1 (2016).

[29] Mohammad Ramzan Parra, Fozia Z. Haque, J. Mater. Res. Tech. **3**(4), 363 (2014).

[30] P. Laokul, S. Arthanl, S. Maensiri, E. Swatsitang, J. Supercond. Nov. Magn. **28**, 2483 (2015).

[31] J. P. Singhal, A. R. Ray, Biomaterials **23**, 1139 (2002).

[32] K. Pal, S. Bag, S. Pal, J. Porous Mater. **15**, 53 (2008).

[33] M. Choimet, H. M. Kim, J. Min Oh, A. Tourrette, C. Drouet, Colloids and Surfaces B: Biointerfaces **145,** 87 (2016).

[34] T. A. Tabish, M. N. Ashiq, M. A. Ullah, S. Iqbal, M. Latif, M. Ali et al., Kor. J. Chem. Eng. **33**, 2222 (2016).

[35] K. Deori, S. Kumar Ujjain, R. K. Sharma, S. Deka, ACS Appl Mater Interfaces **5**, 10665 (2013).

[36] E. Laouini, J. Douch, M. Hamdani, Y. Berghoute, M. H. Mendonca, M. I. S. Pereira et al., J. Appl. Electrochem. **41,** 731 (2011).

[37] S. Ren, X. Zhao, R. Chen, M. Fichtner, J. Power Sources **260**, 205 (2014).

[38] C. I. Nlebedim, Y. Melikhov, D. C. Jiles, J. Appl. Phy. **115**, 043903 (2014).

[39] E. Mazario, M. P. Morales, R. Galindo, P. Herrasti, N. Menendez, Journal of Alloys and Compounds **536S**, S222 (2012).

[40] G. Bulai, L. Diamandescu, I. Dumitru, S. Gurlui, M. Feder, O. F. Caltun, J. Magn. Mag. Mater. **390**, 123 (2015).

[41] T. Slatineanu, A. Iordan, V. Oancea, M. N. Palamaru, I. Dumitru, C. P. Constantin et al., Mater. Sci. Eng. B **178**(16), 1040 (2013).

*Corresponding authors: gaja.nanotech@gmail.com
                        sgokulraj@gmail.com